Biocatalysis and Agricultural Biotechnology 39 (2022) 102258

Contents lists available at ScienceDirect

Biocatalysis and Agricultural Biotechnology

journal homepage: www.elsevier.com/locate/bab

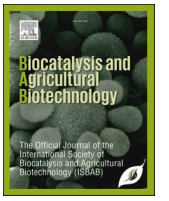

Synthesis of biocompatible Fe_3O_4 and MnO_2 nanoparticles for enhanced tuberization in potato (*Solanum tuberosum* L.)

Neha Joshi, Ph.D [a], Abhishek Pathak, M.Sc [a], Devanshi Chandel Upadhyaya, Ph.D [a], Suresh Babu Naidu Krishna, Ph.D [b], Chandrama Prakash Upadhyay, Ph.D [a,*]

[a] *Laboratory of Plant Molecular Biology, Department of Biotechnology, Dr. Harisingh Gour Central University, Sagar-470003, Madhya Pradesh, India*

[b] *Durban Technological University, Durban, South Africa*

ARTICLE INFO

Keywords:
Metal oxide nanoparticles
Nano-nutrients
Lipoxygenase
Cytosolic Ca^{+2}
Molecular analysis
Tuber yield

ABSTRACT

Iron oxide (Fe_3O_4) and manganese dioxide (MnO_2) Nanoparticles (NPs) were synthesized via green synthesis approach using beetroot (*Beta vulgaris*) leaf extract and evaluated as nanofertilizer for studies of *In-vitro* microtuberization of potato. Successfully biogenesis of NPs were demonstrated through UV–visible spectroscopy, FTIR, XRD, SEM-EDX, and TEM analysis. *In-vitro* micortuberization analysis, single nodal explants of potato were placed on media (Murashige-Skoog plant growth medium devoid of original Fe and Mn salt) added with different concentrations of metal oxide-NPs, and physiological, biochemical and molecular changes were observed via using standard methods. The interaction of the NPs with the nodal explants significantly induced early tuber induction and tuber growth upon application of Fe_3O_4NPs (4.0 mg L^{-1}) and MnO_2NPs (1.0 mg L^{-1}) in comparison to untreated potato tissues. Molecular analysis of potato tissues revealed enhanced expression of primary tuber inducing genes viz. Calcium-Dependent Protein Kinases (*StCDPK*), Calmodulin (*StCaM1*), and Lipoxygenase (*StLOX*) enzyme activity show a positive correlation of tuber induction with added NPs. Further elemental analysis via EDX exhibited that the addition of biocompatible metal oxide NPs in the growth media induced the cytosolic Ca^{+2} burst leading to enhanced expression of major tuber induction pathway genes resulting in early and enhanced potato tuberization. Absorption of metal-oxide NPs in microtubers was evaluated by FTIR and EDX mapping. This study is the first report on the molecular mechanism involved in regulating NPs induced the potato tuberization under *In-vitro* conditions. The study also indicated that application of the metal-oxide NPs as nano-nutrient to enhanced potato microtuber production.

1. Introduction

Nanotechnology has come to light as the 6th revolutionary science of craft after the green and biotechnology revolution. The potential benefits of nanotechnology are enormous in cosmetic, pharmaceuticals, food processing, and textile industries. Among

Abbreviations: NPs, Nanoparticles; CaM, Calmodulin proteins; LOX, Lipoxygenase; Fe_3O_4NPs, Iron oxide nanoparticles; MnO_2NPs, Manganesh oxide nanoparticles; BLAE, Beetroot leaf aqueous extract.

* Corresponding author.

E-mail addresses: jneha191@gmail.com (N. Joshi), Pthkabhi@gmail.com (A. Pathak), devanshiupadhyay@gmail.com (D. Chandel Upadhyaya), sureshk@dut.ac.za (S.B. Naidu Krishna), cpupadhyay@dhsgsu.edu.in (C.P. Upadhyay).

https://doi.org/10.1016/j.bcab.2021.102258
Received 8 May 2021; Received in revised form 28 November 2021; Accepted 17 December 2021

Available online 20 December 2021

others, it has great potential in the agriculture field, especially; nanoparticles (NPs) as micro-nutrients delivery systems could bring crop nutrients efficiently and timely due to their unique physio-chemical properties. Various types of nano-size products are already in the market being used for many applications, so the negative effect of NPs and molecular interactions between NPs and plants is receiving significant interest. In this context, nano-toxicology is an up and coming area of research (Singh et al., 2019). Therefore, it is paramount to prove that NPs fabrication is eco-friendly before being used in agriculture applications (Saratale et al., 2018; Fatima et al., 2021). Hence, the green chemistry principle offers the synthesis of metal NPs utilizing the natural resource, non-hazardous substances. The plant-mediated green synthesis is now widespread and preferred over other methods for the synthesis of various metal oxide NPs, due to its higher reactivity, small size and large surface area for promoting the development of eco-friendly and sustainable farming (Saratale et al., 2018; Khalil et al., 2021). The NPs have been well recognized to interact with the living system. Interaction of NPs with the biomolecules depends on their size, core composition, shape, surface properties, purity, stability, and mode of synthesis of NPs (Singh et al., 2018; Sanzari et al., 2019).

The interactions of metal NPs exhibited positive and negative impacts on the plant's development. The positive impact of NPs interactions with plants cell are enormous, which include the improvement in seed germination, seedling elongation, shoot and root length of plants, photosynthetic activity, change in the uptake of nutrient, thus triggering enhanced plant growth and biomass (Marslin et al., 2017; Hamza, 2019). The essential micro-elements as nano-nutrients including iron (Fe), manganese (Mn), boron (B), copper (Cu), zinc (Zn), and molybdenum (Mo) play an essential role in plant growth, development, and productivity at an optimum concentration. Among these microelements, the role of Fe and Mn have been specially recognized, which play an essential role as an enzyme cofactor of photosynthesis and other metabolic processes, including the enzymatic removal of reactive oxygen species (ROS) (Sidhu et al., 2019; Alejandro et al., 2020; Shi et al., 2020). It has been reported that MnO and FeO NPs as potential nanofertilzer found to be effective for the increasing plants growth and development via modulating antioxidant machinery. (Pradhan et al., 2013; Elmer and White, 2016; Dimkpa et al., 2018; Rui et al., 2016; Moradbeygi et al., 2020; Karunakaran et al., 2017; Liu et al., 2020). Multi-functional properties of Fe and Mn oxide NPs and their biocompatibility in metabolism encourage choosing these NPs in the present study. Nanotechnology has been applied especially in tissue culture for studies of improved crops growth and yield as well as biochemical and molecular changes behind these interaction (Tariq et al., 2020).

The potato (*Solanum tuberosum* L.) is the third most important food crop after wheat and rice. India is the second-largest producer country of potatoes globally after China (Hill et al., 2021). Therefore, careful nutrient management is very important to get maximum yield. Potato tubers are formed via swelling of the underground stem into stolon, subsequently growing as an inflated structure like tuber due to storage of starch, also has chances of direct uptake of nanoparticles from medium, thus manipulating the tuberization. To the author's knowledge, only few studies have shown the effect of NPs under *In-vitro* conditions such as the application of Cobalt NPs (CoNPs) with the presence of sucrose and ABA in MS media induced tuber growth and yield (Hamza, 2019), and pectin tagged nano-silver effective for microtuberization (Abedini et al., 2020).There is no report till date on understanding the impact of Fe and Mn oxide NPs on tuberization efficacy of potato. In lieu of above discussion, the current work describes a green synthesis of stable, biocompatible Fe_3O_4 and MnO_2 NPs using beetroot (*Beta vulgaris* L.) leaves aqueous extracts as a reducing agent. The molecular and biochemical studies were also done to unearth the interaction of the metal oxide NPs with the potato tissues leading to induction of tuber formation under *In-vitro* conditions.

2. Material and methods

2.1. Green synthesis of metal oxide nanoparticles

2.1.1. Preparation of beetroot leave extract

Younger leaves (100 mg) of beetroot (*Beta vulgaris* L.) were dried and crushed to a fine powder and transferred to Erlenmeyer flasks containing double distilled water (100 mL). The mixture was boiled for 30 min and filtered through Whatman filter paper No. 1 to collect the aqueous filtrate, stored at 4 °C. The filtrate was referred to as beetroot leaf aqueous extract (BLAE) and used as a reducing agent for synthesis of Fe and Mn metal oxide NPs.

2.1.2. Synthesis of metal oxide NPs

The solution containing (45 mL of 20.0 mM $FeCl_36H_2O$, and 45 mL of 10 mM $FeCl_24H_2O$ Sigma-Aldrich, USA) were taken to a flask and 10 mL of the BLAE was added to it. The mixture was heated at 80 °C for 5–10 min on water bath. The change in colour of solution indicated the completion of reaction and the synthesis of Fe_3O_4. Similarly, MnO_2 NPs were synthesized taking an aqueous solution of potassium permanganate (2.0 mM, 90 ml $KMnO_4$, Sigma-Aldrich) in the flask, and 10 mL of BLAE was added to it. This solution mixture was heated at 80°C on the water bath to initiate reduction process. Completing the reaction was indicated by a change in colour and the synthesis of MnO_2 NPs. At the same time, synthesis of NPs was monitored via a change in absorption spectra from different time intervals at 200–600 nm wavelength using UV–Visible spectrophotometer (UV-1800, Shimadzu, Japan). The colloidal suspensions obtained upon completion of reduction reaction were then centrifuged and washed several times with ethanol and dried at 40 °C. The purified dried powder of the Fe_3O_4 and MnO_2 NPs were further characterized and used in experiments.

2.2. Characterization of metal oxide NPs

The Fourier-Transform Infra-Red (FTIR) spectroscopic measurement of electromagnetic radiation were recorded through FTIR-BRUKER Tensor 37 (Bruker, USA) with wavelengths within the mid-infrared region (4000–400 cm^{-1}) operating at a resolution of 4.0 cm^{-1}.The crystalline structure and phase purity of the biogenic iron and manganese oxide NPs were identified by X-ray diffraction measurement (XRD, Model D8 Advance BRUKER, USA) equipped with Cu-kα (1.54060 Å) radiation at 2θ angle pattern with scanning

in the range of 5°–100° (Joshi et al., 2019).

The shape and size distribution of Fe and Mn oxide NPs were quantified using high-resolution Scanning Electron Microscopy (SEM, Nova Nanosem 450) operated at an accelerating voltage of 20 kV (Joshi et al., 2019). The elemental content of the oxide NPs was analyzed using SEM data equipped with EDS quantification software. The size and internal morphology of green synthesized NPs were also determined using Transmission Electron Microscopy (TEM, Talos F200X G2, UK). The TEM grid was prepared by loading 1.0 μL NPs solution on the carbon-coated copper grid. The samples dried under the lamp, and images were taken using an accelerating voltage 200 kV (Joshi et al., 2018).

2.3. *In-vitro tuberization with supplementation of metal oxide NPs in the growth medium*

The potato (*Solanum tuberosum* L) variety Kufri jyoti obtained from Central Potato Research Station, India, were used for this study. Tuberization experiments were done using a single nodal segment collected from 4 to 5 weeks old plants. The nodal segments were placed on the MS (Murashige–Skoog) medium (Murashige and Skoog, 1962), devoid of its original constituent of Fe and Mn salts containing 7% sucrose, 0.8% agar with pH 5.8 supplemented with various concentrations of either Fe and Mn oxide NPs (0 ppm–6 ppm concentrations). The NPs were added in the MS medium by sonicating the NPs aqueous solution to distribute evenly into the medium. The cultures were incubated under continuous dark with 60 ± 5% relative humidity at 18±2 °C, following the standard protocol (Upadhyaya et al., 2016). The MS medium devoid of NPs served as an experimental control. An independent set of experiments used as the negative control where the MS medium was added with green synthesized silver nanoparticles (Ag NPs) (Particle size 40–60 nm according to SEM analysis (Joshi et al., 2019), and TEM image of Ag NPs represented in the Supplementary Fig. 3) which inhibit the tuberization process. The MS medium (with 7% sucrose) supplemented with 9.0 mM of $CaCl_2$ was also used in the study as a positive control, as the application of Ca^{+2} in the medium has already been shown to induce efficient *In-vitro* tuberization (Upadhyaya et al., 2016). The growth of developing buds was observed daily by measuring the length of stolon tuber induction period and the width of tubers by determining the frequency of tuberization. The data of each culture condition was taken as average of uniformly grown tubers, and stolon were collected separately for 30 days, depending on the sample type. The stolon developed first on the node hence collected first and so on, each treatment consisted of 50 nodal segments, and the experiment was repeated thrice with a total of 150 explants.

2.4. *Evaluation of NPs uptake by plant tissues*

Accumulation of Fe and Mn NPs in the treated and untreated microtuber tissues were analyzed using the non-quantities simple techniques such as FTIR spectroscopy and SEM-EDS mapping. The dried tuber tissues's powder spectrum was recorded through FTIR-BRUKER Tensor 37 (Bruker, USA) via the transmittance mode over the range of 400–4000 cm^{-1} operating at a resolution of 4.0 cm^{-1} (Boutchuen et al., 2019).

Elemental analysis of metal oxide NPs treated and untreated *In-vitro* grown tuber samples were examined separately under Scanning Electron Microscopy (SEM), (Model- Nova Nanosem 450) equipped with Energy Dispersive Spectrum (EDS) analysis software. The samples were dried and crushed to a fine powder poured onto conductive carbon coated adhesive tape followed by gold coating, and further analysis was done to confirm the presence of Fe and Mn NPs in the treated tuber samples (Shankramma et al., 2016).

2.5. *Expression analysis of signalling pathways genes for tuberization*

The calcium-dependent protein kinases (*StCDPK*), calmodulin proteins (*StCaM*) and lipoxygenase (*StLOX*) cascade are recognized as major signalling pathway genes regulating the potato tuberization. Total RNA was isolated from the stolon and tubers, using the TriZol™ reagent (Invitrogen, USA) following the standard protocol. The cDNA synthesis was done using SuperScript™ Reverse Transcriptase enzyme (Invitrogen, USA) as per manufacturer's instructions. The cDNA synthesized was used as a template for the gene expression analysis in a Real-Time PCR system with the gene-specific primers (Supplementary Table 1) using SYBR Green Supermix (Applied Biosystems, USA) as per the manufacturer's instructions.

The actin gene-specific primers were used as an internal amplification control where the proportional threshold (Ct) values were normalized to actin gene for analyzing the comparative expression.

The RT-PCR (reverse transcriptase PCR) reactions were also performed in a thermal cycler (Bio-Rad, USA) in a 25 μL reaction mixture using the cDNA (1.0 μL) added with 10 pmol of each primer and 0.3 U of Taq-DNA polymerase (Invitrogen, USA) following standard protocol. Reaction products were separated on 1.2% agarose gel stained with ethidium bromide and visualized under UV light (VILBER BIO-PRINT UV).

2.6. *Estimation of lipoxygenase (LOX) enzyme activity*

The Lipoxygenase enzyme activities were quantified from collected stolon and tuber tissues growing under *In-vitro* following the procedure as reported (Gökmen et al., 2002) Total protein extraction and quantification were done using the standard protocol (Bradford, 1976). The LOX enzyme assay was performed using a substrate solution prepared by mixing 2.0 mL of potassium phosphate buffer (0.1 M; pH 6.0), 2.0 μL of Tween-20 and 2.0 μL of pure linoleic acid (Sigma, USA). A gentle stream of air passed through the solution for aeration, and the reaction was initiated by adding 100 μL of crude protein extract to the solution. The blank reaction consisted of a substrate solution (2.0 mL) added with distilled water (100 μL). The enzyme activity was estimated using spectrophotometric monitoring for the synthesis of hydroperoxide due to the presence of a conjugated hydroperoxydiene moiety. One unit of LOX activity was defined as an increase in absorbance of 0.001 at 234 nm min^{-1} mg^{-1} of protein under assay conditions.

2.7. Statistical analysis

The data were analyzed with the one-way analysis of variance (ANOVA) using SPSS software (version Statistics V26, Windows XP). Tukey's *t*-test at $P < 0.05$ was used for multiple comparisons of mean.

3. Results and discussion

3.1. Green synthesis of the Fe_3O_4 and MnO_2 NPs

A consistent and eco-friendly method for the synthesis of NPs is of the utmost importance to expand their applications in agriculture fields (Singh et al., 2018; Saratale et al., 2018). The study focused on synthesis of Fe_3O_4 and MnO_2NPs using BLAE. As shown in (Supplementary Fig. 1), the colour of the Fe^{3+}/Fe^{2+} and BLAE solutions changed rapidly from light yellow to dark brown, indicating the completion of reduction reaction and synthesis of iron oxide NPs (Supplementary Fig. 1 A). Similarly, the time course of reducing the $KMnO_4$ and the synthesis of the MnO_2 NP using the BLAE was monitored by the change in colour from purple to yellow-brown and finally to black that indicated the reduction reaction well synthesis of manganese oxide NPs (Supplementary Fig. 1 B).

The spectrophotometric absorbance of BLAE showed a peak at 220 nm, and a slight shift to 260 nm indicated the presence of phenolic compounds in the aqueous extract, which induced the reduction of parent material resulting in the genesis of metal oxide NPs. The absorbance peak at 270 and 280 nm confirmed the presence of Fe_3O_4 and MnO_2 NPs, respectively (Supplementary Fig. 1 C). The BLAE have been reported to contain several bioactive components, including the betalains (betanin and isobetanin), phenolic amides as well as flavonoids (betagarin, betavulgarin, cochliophilin A) with active organic groups such as hydroxyl, ketones, and aldehydes (Chhikara et al., 2019). These phyto-constituents promoted the reduction reactions to develop stable iron oxide NPs via capping action. Initially, the Fe(III)/Fe(II) hydrolyzed to form iron hydroxide and releases H^+ ions; after that, iron hydroxide was partially reduced by BLAE to form Fe_3O_4 NPs aldehyde groups are oxidized to the corresponding acids.

Similarly, the MnO_2 NP was also synthesized using the BLAE. A possible explanation for this may be that the phytochemicals present in the BLAE acted as reducing and stabilizing agents. Manganese is a paramagnetic metal that oxidizes quickly, resulting in the highly agglomerated particles reducing its further bioactivity. The permanent black colour's appearance also indicated the completion of reduction reaction and synthesis of stabilized MnO_2 NPs due to the presence of the plant-based capping agent. Green synthesized inorganic metallic nanoparticles have emerged as promising material due to their higher stability and lower toxicity for eukaryotic cells as compared to organic material. Therefore, green synthesized metal oxide NPs were considered for the study. Metal oxide NPs has been used as skincare commodities, antibacterial agents, biomedical, food-additive industries, and agriculture application (Khan et al., 2017, 2020; Singh et al., 2018; Rizwan et al., 2019; Liu et al., 2020; Nazri and Sapawe, 2020; Umavathi et al., 2021). The proposed green synthesis method of metal oxide NPs was not reported earlier and found to be effective and highly reproducible.

3.2. Characterization of metal oxide NPs

3.2.1. FTIR and XRD analysis

The FTIR spectra of leaf extract and Fe and Mn oxide NPs were recorded to find out the biochemical moieties involved in the synthesis of metal oxide NPs. The FTIR spectra of BLAE and NPs are represented in Fig. 1 A-C. The presence of betanidine and its phenolic functional groups in BLAE and NPs were depicted in the spectra. The absorption bands at 3500 cm^{-1} indicated the presence of the phenolic-OH group. Similarly, absorption bands at 2700 cm^{-1}, 2610 cm^{-1}, 1755 cm^{-1}, and 1170 cm^{1} peak represented C–H, CHO, O–H, and C–O groups. Peaks at 1521 cm^{-1} and 1347 cm^{-1} also confirmed the presence of N–O and N–H groups. The appearance of

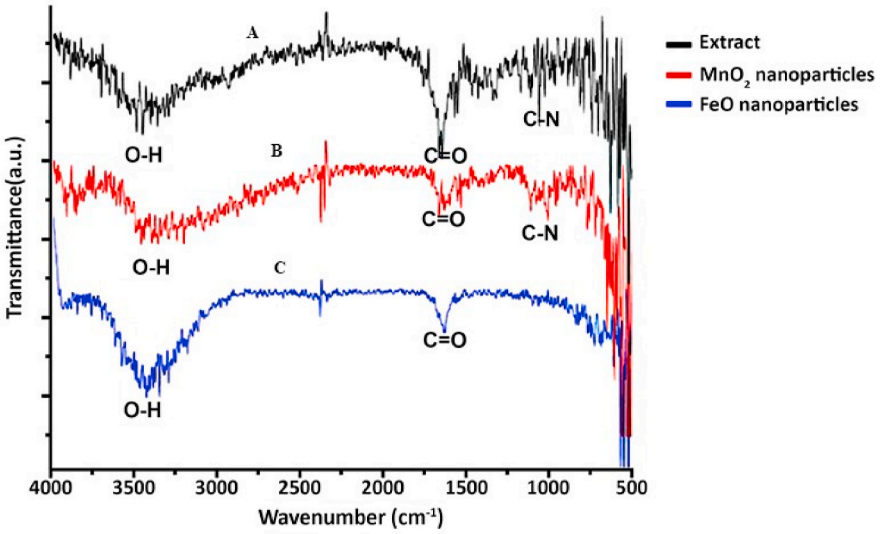

Fig. 1. FTIR spectra of Beetroot leaf extract and metal oxide NPs. (**A**) Beetroot leaf aqueous extract, (**B**) MnO2 NPs and (**C**) Fe_3O_4 NPs.

absorption bands in the FTIR spectra at 575 cm^{-1} may be due to the formation of Fe–O bonds and at 515 cm^{-1} correspond to the Mn–O bond, which confirmed the synthesis of metal oxide NPs via reduction of BLAE (Mourdikoudis et al., 2018; Souri et al., 2018). Besides, the disappearance of C═O, C–N groups in the BLAE indicated that these groups were involved in reducing metal oxide NPs. The intense –OH group peak in the IR spectra of the NPs showed that the hydroxyl groups moieties such as betalains, betanidin, and betanin acted as a stabilizing agent during the synthesis of the NPs.

The XRD patterns of green synthesized Fe and Mn oxide NPs are represented as Fig. 2 A and B. The evident peaks of Fe_3O_4 and MnO_2 oxide NPs correspond to an orthorhombic and tetragonal structure. The intense XRD peak of Fe_3O_4NPs observed at 31.9^O, 33.4^O, 35.5^O, 38.5^O and 47.5^O correspond to 100, 023,102, 040, and 132 defined the NPs Bragg's refection according to JCPDS card file 89–6466. The XRD peak of MnO_2 NPs at 20.5^O, 26.2^O, $28.5^{O,}$ and 35.5^O correspond to 200, 220, 002 and 312 defined NPs Bragg's refection according to JCPDS card file-02-0567. The banding of the Bragg's peaks indicated the successful synthesis and crystalline nature of metal oxide NPs.

3.2.2. *Electron microscopy and elemental content analysis*

The shape and size of metal oxide NPs were confirmed by electron microscopy. The SEM images clearly showed nano-size (around 20–56 nm for Fe_3O_4 NPs and 9–30 nm for MnO_2 NPs) (Fig. 3 A and B). Besides, the TEM image analysis also demonstrated the spherical shape and nano in structure (average particles size was around 10.6 ± 2.24 for Fe_3O_4 NPs and 6.3 ± 1.17 for MnO_2 NPs) with a small degree of agglomeration (Fig. 3 C and D).

The Energy Dispersive Spectroscopic (EDS) method was used to determine the elemental composition and stoichiometry of both kinds of green synthesized metal oxide NPs. The spectral signals of iron, manganese and oxygen from the Fe_3O_4 and MnO_2 NPs were detected. Peak around 0.5 KeV, 6.0 KeV and 6.5 KeV correspond to the bonding energy of oxygen, manganese, and iron, respectively. Other signals with varied energy may be arising from the bioactive molecules of the BLAE. The weight percentage (W%) of elements present in the metal oxide NPs as shown in the figure along with EDS data of corresponding NPs (Fig. 3 E and F).

3.3. *Effect of metal oxide NPs on in-vitro tuberization of potato*

The supplementation of green synthesized Fe or Mn oxide NPs in MS medium devoid of its original Fe and Mn salt resulted in early stolons formation and subsequent tuber induction on the nodal explants within 5–8 days of culture. Delayed *In-vitro* tuber induction was observed (within 12–14 days) in the case of the untreated control explants (MS media without NPs). The addition of Fe_3O_4 NPs in the medium at 4.0 ppm concentrations resulted in tuber induction within 7–8 days; while the supplementing MnO_2 NPs at 1.0 ppm resulted in early tuber induction within 5–6 days (Supplementary Fig. 2). Thus, the period of tuber induction reduced to 5–8 days with the NPs treated plant tissues with respect to control explants. We could observe delayed and deformed or no tubers induction on the stolons in the MS medium supplemented with 1.0 ppm Ag NPs concentrations due to its cytotoxic effect on the tissues. Thus, adding either metal oxide NPs in the MS medium resulted in comparatively early tuber induction, increased tuber size, average tuber weight, and yield. Interestingly, supplementation of MnO_2 NPs to the MS medium performed better in early tuber induction and overall tuber yield (Table 1).

Nanomaterials have been reported to influence key life events of the plants, including seed germination, seedling vigour, root initiation, growth and development, photosynthesis, and flowering via a mechanism of altering the gene expression involved in cell biosynthesis, cell organization, electron transport pathways and stress responses (Acharya and Pal, 2020; Marslin et al., 2017; Fouad and Hafez, 2018; Mozafari et al., 2018a, b; Zhao et al., 2020; Fatima et al., 2021; Liu et al., 2020). It has been reported that addition of Co NPs in tuber inducing medium enhanced the microtuberization of potato (Hamza, 2019). The green synthesized Fe, and Mn oxide NPs have shown the positive impact on maize seedling germination, root development, and fresh weight, it has been used as an efficient nanofertilizer for crops growth (de França Bettencourt et al., 2020). Induction of *In-vitro* potato tuberization by the NPs in this study might be due to its elicitor action and interaction with various cellular factors triggering the hypersensitive responses of various

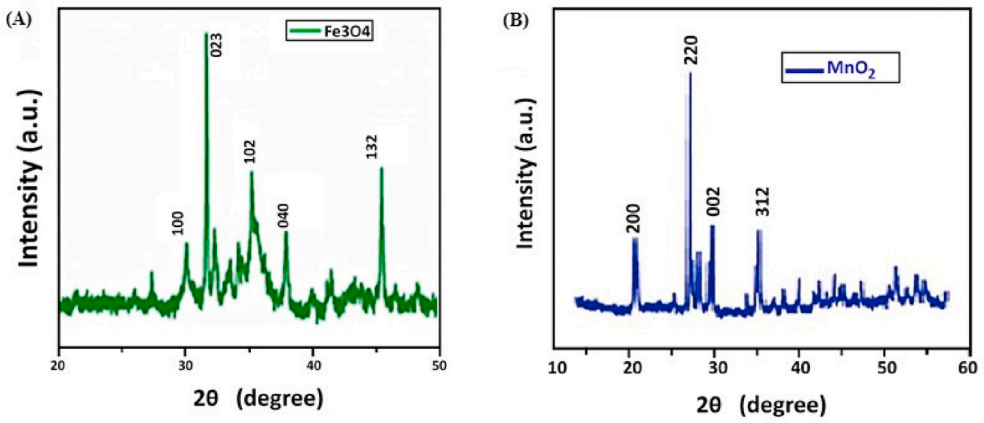

Fig. 2. X-ray diffraction patterns of metal oxide NPs (**A**) Fe_3O_4 NPs and (**B**) MnO_2 NPs.

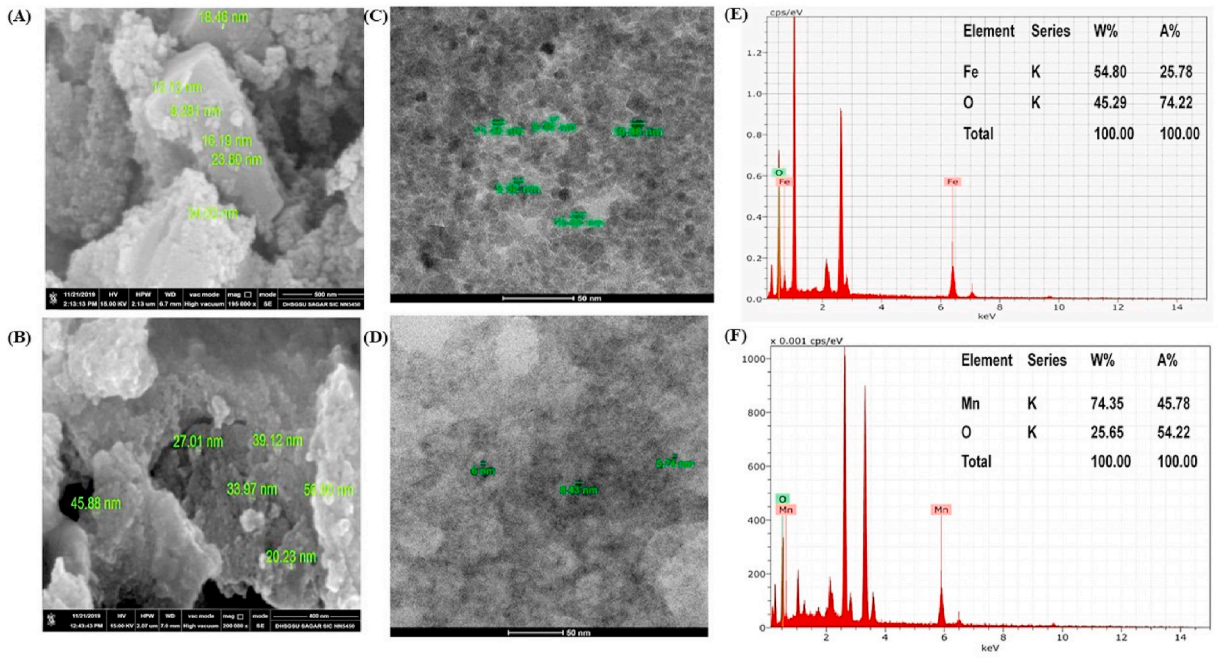

Fig. 3. Electron microscopy image and EDS analysis of metal oxide NPs. (A) SEM image of Fe_3O_4 NPs **(B)** SEM image of MnO_2 NPs **(C)** TEM image of Fe_3O_4 NPs **(D)** TEM image of MnO_2 NPs **(E)** EDS analysis of Fe_3O_4 NPs **(F)** EDS analysis of MnO_2 NPs.

Table 1
Influence of application of different NPs in MS medium on *In-vitro* tuberization. of potato.

Treatments	Control	Fe_3O_4 NPs				MnO_2 NPs				Ag NPs	$Cacl_2$
Concentration	**0.0 ppm**	**1.0 ppm**	**2.0 ppm**	**4.0 ppm**	**6.0 ppm**	**0.5 ppm**	**1.0 ppm**	**1.5 ppm**	**2.0 ppm**	**1.0 ppm**	**9 mM**
No. of Nodal explants	150	150	150	**150**	150	150	**150**	150	150	150	**150**
No. of stolon induced on nodal tissues	118 ± 4.5c	116 ± 5.5c	125 ± 4.2 ab	**130 ± 5.5 a**	82 ± 2.5d	122 ± 5.5c	**139 ± 4.2a**	118 ± 5.5b	110 ± 2.5cd	42 ± 2.2e	**144 ± 2.2a**
No. of stolon inducing tubers	88 ± 3.5c	92 ± 2.2c	107 ± 3.6b	**116 ± 4.5a**	75 ± 1.5c	96 ± 3.6c	**128 ± 4.5a**	96 ± 5.5b	72 ± 4.2 cd	14 ± 1.5e	**134 ± 4.2a**
Days to tuber initiation	12-14c	10–12bc	9–10b	**7-8a**	11-13c	8-10c	**5-6a**	5-7 ab	9–11cd	18-20e	**4-5a**
Av. tuber size (mm)	2.50 ± 0.01c	4.40 ± 0.04c	5.51 ± 0.10b	**6.12 ± 0.10a**	5.1 ± 0.04 ab	4.55 ± 0.11c	**7.16 ± 0.10a**	5.55 ± 0.11b	3.15 ± 0.12cd	2.20 ± 0.11e	**8.24 ± 0.22a**
Av. tuber wt. (g)	0.36 ± 0.02c	0.42 ± 0.04c	0.60 ± 0.02b	**0.75 ± 0.04a**	0.31 ± 0.02d	0.52 ± 0.10c	**0.82 ± 0.10a**	0.682 ± 0.12b	0.42 ± 0.30cd	0.29 ± 0.02e	**0.99 ± 0.12a**
Av. Tuber yield (g)	24.2 ± 0.36d	57.2 ± 0.14c	77.2 ± 0.16b	**85.2 ± 0.16a**	36.2 ± 0.16d	68.2 ± 0.22c	**102.5 ± 0.20a**	75.2 ± 0.22b	47.2 ± 0.21cd	11.2 ± 0.16e	**110 ± 4.2a**

Basal medium: MS medium (without Fe and Mn salt + respective metal oxide NPs). The values are presented as the mean ± SE of three replicates. Number of explants inoculated per treatment: 50; Average tuber yield was calculated per treatment containing 50 explants. Different letters in the table indicate that mean values are significant between control and NPs treated plants ($p < 0.05$) after Duncan's multiple range tests.

metabolic pathways. It has already been hypothesized in cellular studies that the NPs interfere with cell metabolism through the binding with Ca^{+2} receptors, calcium ion channels, Ca^{+2}/Na^{+} pumps resulting in alteration of intracellular Ca^{+2}, and functional modulation of various calcium-dependent protein kinases (Rastogi et al., 2017; Marslin et al., 2017; Mirzajani et al., 2014).The addition of calcium under the In-vitro and In-vivo conditions induces the plant morphological characteristics, including the tuber induction and yield, which emphasized that the calcium ions play an important role in the tuberization pathway regulation (Upadhyaya et al., 2016; Seifu and Deneke, 2017). Elemental data analysis of the NPs treated tubers indicated enhanced Ca^{2+} ions content (Fig. 5 and Supplementary Fig. 4). Therefore, it indicated that the addition of metal oxide NPs in the medium absorbed by the plant tissues, which might alter the cytosolic Ca^{+2} concentrations that positively induced the calcium signalling pathway genes regulating the tuber formation resulting in enhanced potato tuberization.

3.4. Evaluation of NPs uptake by plant tissue

The FTIR, and SEM equipped with EDX analysis of the treated and untreated microtuber samples were done for comparative quantification of absorbed and accumulated metal oxide NPs by plants. The untreated tuber sample exhibited the FTIR spectral peak

ranging from 3000 cm^{-1} to 4000 cm^{-1} representing the O–H and N–H groups; the spectra peak at 2354 cm^{-1} exhibited O═C═O stretching; the peak at 1700 cm^{-1} to 1200 cm^{-1} attributed to C═O stretch and 1100 to 500 cm^{-1} in the fingerprinting region owing to the starch (Basiak et al., 2018). These sections were visualized in the FTIR spectra of all the NPs treated and untreated tuber samples. However, the tubers treated with Fe and Mn oxide NPs showed the instance peak at 2357 cm^{-1} and 580 cm^{-1}, respectively (Fig. 4 B and C), absent in the untreated tubers samples (Fig. 4 A). This data represented the internalization of NPs in the tuber tissues.

The SEM images and their corresponding EDX spectral data of NPs treated tuber samples are represented in Fig. 5. In addition, Supplementary Fig. 4 represented EDX elemental mapping of corresponding elements (Fe, Mn, and Ca) presence in the *In-vitro* grown micro-tubers. The SEM image and the EDX elemental analysis of NPs treated tuber tissues showed a slightly higher content of Fe and Mn element within the *In-vitro* grown micro-tubers (Fig. 5 B and C, Supplementary Fig. 4), while lower metal content was observed in the untreated tissues (Fig. 5 A, and Supplementary Fig. 4).

The mapping data also indicated enhanced Ca^{+2} ions content in the NPs treated tuber samples compared to the untreated tuber samples (Fig. 5 and Supplementary Fig. 4). This data also corroborated with the enhanced gene expression of the calcium signalling pathway genes (*St CaM1*, *St CDPK*) and the tuber inducing *St LOX* genes in the plant tissues, thus triggering enhanced tuber induction.

This study utilized sample non-quantification techniques such as FTIR and SEM- EDX mapping for the comparative study of accumulated metal oxide NPs. (Jeyasubramanian et al., 2016; Shankramma et al., 2016; Palchoudhury et al., 2018; Yan and Chen, 2018; Boutchuen et al., 2019).

The FTIR and SEM-EDX mapping data of NPs treated tuber tissue samples confirmed the plant's absorbance and transport of the Fe3O4 and MnO2 NPs. Similarly, The FTIR characterization method has been used to analyze FeO NPs transport in the legume plants, and quantification of iron oxide NPs has been done by the SEM-EDX analysis in tomato root, respectively (Boutchuen et al., 2019; Shankramma et al., 2016).

3.5. *Expression analysis of the signalling pathways genes involved in tuberization*

To investigate the possible mechanism of NPs induced *In-vitro* tuberization in potato, the quantitative Real-time PCR (q-PCR) expression analyses were done with the Ca^{2+} dependent tuberization specific signalling pathways genes, the *St CaM1* and *St CDPK* in particular, as well as the *St LOX* gene. The q-PCR analysis showed an enhanced transcript of the *St CaM1*, *St CDPK* and *St LOX* genes in stoloniferous shoot growing on MS medium with Fe_3O_4 NPs (4.0 ppm), MnO_2 NPs (1.0 ppm) and $CaCl_2$ (9.0 ppm) (Fig. 6 A). However, their expressions showed a decreasing pattern in initial and developed tubers (Fig. 6 B). These results were further corroborated by qualitative reverse transcriptase PCR (RT-PCR) analysis which also exhibited enhanced transcript of the above genes in the stolon. The transcript expressions of gene were comparatively higher in stoloniferous shoot growing in the presence of the metal oxide NPs and $CaCl_2$ than the nodal explants kept for tuberization on the MS medium without the NPs (Fig. 6 C).

Increased tuber growth and yield with the supplementation of either of the NPs in the MS medium could also be attributed to phosphorylation of tuberization specific genes leading to enhanced expression of the Ca^{2+} dependent genes, the *StCaM1* and *StCDPK*.

Activation of the gene expression is primarily carried out by a signalling network that triggers the molecular machinery for a particular developmental pathway. Cytosolic Ca^{+2} acts as a second messenger and play an important role in signalling responses to various pathways. Perception of the stimulus (physical/environmental) causes mobilization of Ca^{+2} from its storage sites to cytosol through Ca^{+2} channels leading to an elevation in cytosolic Ca^{+2} concentration. Increase in the cytosolic Ca^{+2} sensed by Ca^{+2}-binding proteins which initiate downstream events leading to changes in gene expression and, therefore, modifying the plant developmental

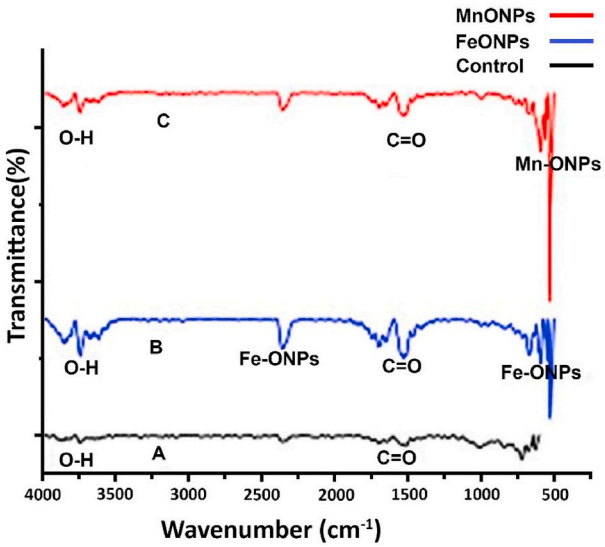

Fig. 4. FTIR spectra of initial tubers tissues in the region 500- 4000 cm^{-1}. **(A)** FTIR spectra of untreated tuber **(B)** FTIR spectra of Fe_3O_4 NPs treated tuber. **(C)** FTIR spectra of MnO_2 NPs treated tuber.

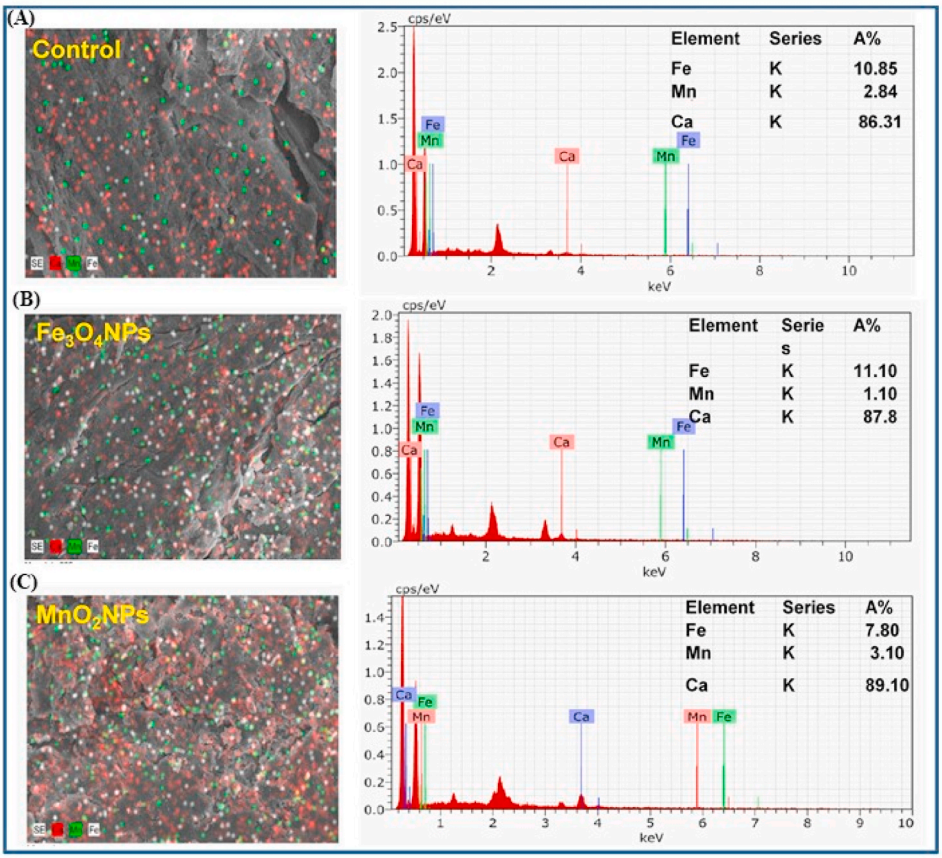

Fig. 5. SEM image and corresponding EDS of *In-vitro* grown potato tubers upon the treatment with Fe and Mn oxide NPs **(A)** Untreated control **(B)**Tubers sample treated with Fe_3O_4 NPs and **(C)** MnO_2 NPs.

phenomenon (Marslin et al., 2017; Bagur and Hajnóczky, 2017; Rastogi et al., 2017 Upadhyaya et al., 2016; Ahmad et al., 2018). It has also been reported that the *St CDPK* may act as a stimulus-response coupler in calcium-regulated processes during tuberization in potato (Upadhyaya et al.,2013, 2016). A Schematic representation describing the possible mechanisms involved in nanoparticles-mediated modulation of potato tuberization pathway is shown in Fig. 7.

3.6. Estimation of lipoxygenase (LOX) activity

An enhanced lipoxygenase (LOX) enzyme activity was observed in the stolons and initial tubers tissues as evident in the enzyme assay (Fig. 8 A and B). The enhanced activity of LOX enzyme is recognized during the potato tuberization (Nam et al., 2005). The LOX enzyme catalyzes lipid peroxidation using the membrane lipid constituents, particularly the polyunsaturated fatty acids such as linolenic acids, which results in the biosynthesis of Jasmonic acid (JA), which is further spontaneously metabolized to tuberonic acid (TA), and tuberonic-acid-glucoside (TAG) with stronger tuber-inducing activities (Koda, 1997; Vincenti et al., 2019). Therefore, early tuber induction increased tuber size and yield in this study could be credited to the higher synthesis of LOX derived metabolites playing a central role in tuberization. In addition, it has been reported that the increase LOX activity also depends upon the gene expression of calcium-dependent proteins such as *StCDPK* and *StCaM1* (Kolomiets et al., 2001; Upadhyaya et al., 2013, 2016). The increased expression of LOX genes in the study also corroborated with the increased LOX activity that triggered tuber formation at the stolon.

4. Conclusion

Metal oxide NPs have been successfully synthesized by ecofriendly, cost effective method. Supplementation of the green synthesized Fe and Mn oxide NPs in the tuberization medium efficiently absorbed by the potato nodal tissues and played an essential role of elicitor, thus induced early tuber formation, tuber size and overall yield per explants. Molecular and biochemical analysis revealed enhanced expression of main calcium-dependent tuberization specific genes, controlling in-plant tuber formation via a series of complex metabolic processes. This is due to nanosize, large surface area to volume ratio, and bioactive moieties on biogenic metal oxide NPs. The above results concluded that applying the metal oxide NPs as nano-nutrient at optimum concentrations played an important role in augmenting enhanced potato micro-tuber yield. Biogenic metal oxide NPs could be a better source for agriculture application as nanofertilizer.

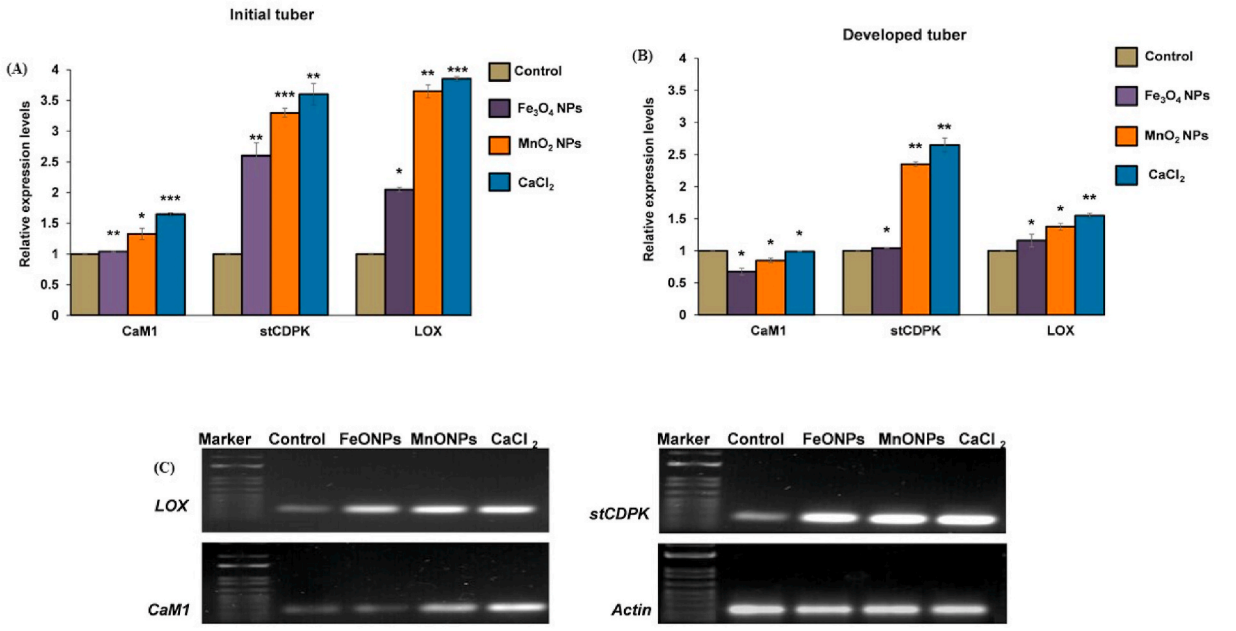

Fig. 6. Expression analysis of *CaM1*, *StCDPK*and *LOX* genes in stolons and initial tuber tissues of potato during tuber development. **(A)**PCR expression analysis of the various gene expressions in the initial tuber tissues. **(B)**q-PCR expression analysis of the various gene expressions in the developed tuber tissues. **(C)**Semi-quantitative RT-PCR expression level of *LOX*, Cam1, and *stCDPK,* genes in initial tuber tissue of potato during tuberization. Actin gene was taken as control internal gene expression Lane in the Gel, Control-without NPs; Fe_3O_4 NPs- 4.0 ppm; MnO_2 NPs- 1.0 ppm; $CaCl_2$- 9 mM. Real Time q-PCR data were analyzed by comparative ΔΔ CT method. Experiments was performed in triplicate and values shown are means ± SD of each treatment. Significant changes are marked with asterisk: * p-value < 0.05, ** p-value <0.01, and *** p-value <0.001.

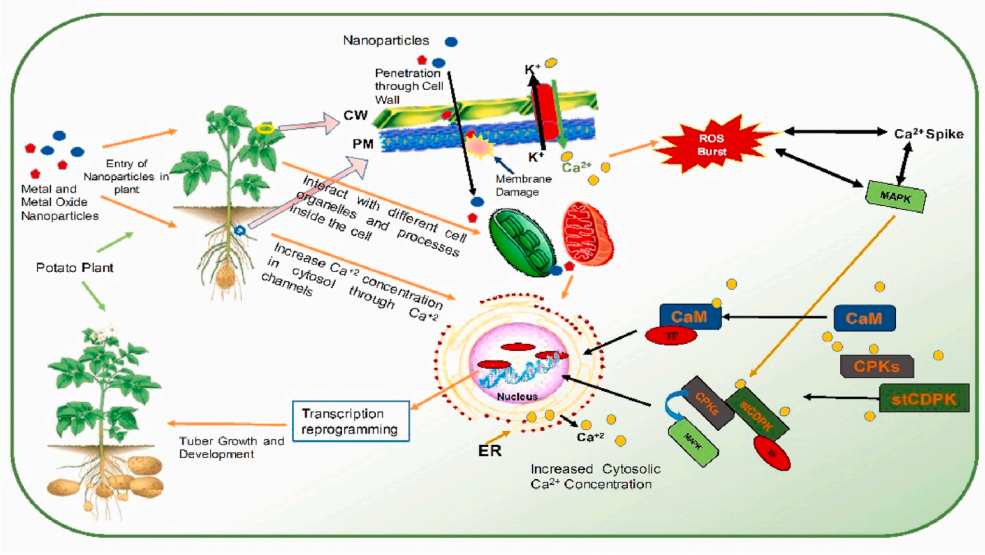

Fig. 7. A possible mechanism involved in nanoparticles interaction with plant and modulation of potato tuberization pathways. Abbreviations: CaM, Calmodulin; stCDPKs/CPKs, Calcium Dependent Protein Kinases; MAPK, Mitogen Activated Protein, Kinase; TF, Transcription Factor; ROS, Reactive Oxygen Species; ER, Endoplasmic Reticulum; CW, Cell Wall; PM, Plasma Membrane.

Declaration of competing interest

I declare that there is no conflict of interest regarding the MS content. I also declare that all the authors have read the final version of this MS. I accept all the terms and conditions of the journal regarding the publication of article.

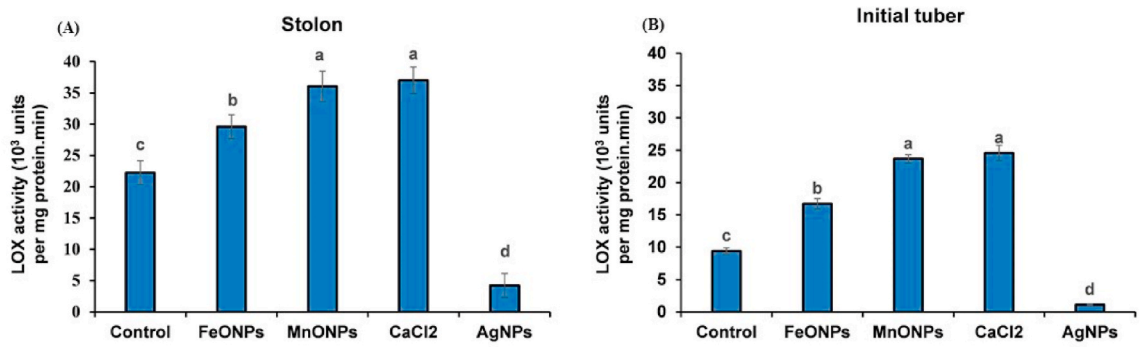

Fig. 8. Lipoxygenase (LOX) enzyme assay in different tuber tissues developed during *In-vitro* tuberization of potato in presence of meta l oxide NPs. **(A)** LOX activity in stolon and **(B)** Initial tuber. Control represents the tuber tissues growing on MS medium in absence of NPs; FeO NPs represents tuber tissues developed on MS medium in presence of 4.0 ppm Fe_3O_4 NPs; MnO NPs represents tuberization in presence of 1.0 ppm MnO_2 NPs; $CaCl_2$ represented the tuberization in presence of 9 mM $CaCl_2$ salt and Ag NPs represent the tuberization in presence of 1.0 ppm Ag NPs in MS medium. The values are presented as the mean ± SEM (standard error means) of three replicates and different lowercase letters on bars indicate statistically significant differences among the treatments at $p < 0.05$ according to tukey's test.

Acknowledgments

Authors are thankful to DST-PURSE funded Sophisticated Instrumentation facility at Dr. Harisingh Gour University, Sagar, Madhya Pradesh, India. We also acknowledge the use of Sophisticated Analytical Instrumentation Facility (SAIF), All India Institute of Medical Sciences (AIIMS), New Delhi for the TEM analysis. NJ acknowledges the fellowship under UGC research fellowship program from Dr Harisingh Gour University, Sagar, Madhya Pradesh, India.

Appendix A. Supplementary data

Supplementary data to this article can be found online at https://doi.org/10.1016/j.bcab.2021.102258.

References

Abedini, M., Motallebi, Azar, A., Zaare, Nahandi, F., Gohari, G., 2020. Application of pectin- tagged nano silver and triacontanol on in vitro microruberization of *Solanum tuberosum* L. Cv. Agria. J. Veg. Sci. 4 (1), 57–70. https://doi.org/10.22034/iuvs.2020.129406.1103.

Acharya, A., Pal, P.K., 2020. Agriculture nanotechnology: translating research outcome to field applications by influencing environmental sustainability. Nano Impact 8, 100232.

Ahmad, P., Abd, Allah, E.F., Alyemeni, M.N., et al., 2018. Exogenous application of calcium to 24-epibrassinosteroid pre-treated tomato seedlings mitigates NaCl toxicity by modifying ascorbate–glutathione cycle and secondary metabolites. Sci. Rep. 8, 13515. https://doi.org/10.1038/s41598-018-31917-1.

Alejandro, S., Holler, S., Meier, B., Peiter, E., 2020. Manganese in plants: from Acquisition to subcellular allocation. Front. Plant Sci. 11 https://doi.org/10.3389/fpls.2020.00300.

Bagur, R., Hajnóczky, G., 2017. Intracellular Ca^{2+} sensing: its role in calcium homeostasis and signaling. Mol. Cell. 66 (6), 780–788, 10.1016/j.molcel.2017.05.028.

Basiak, E., Lenart, A., Debeaufort, F., 2018. How glycerol and water contents affect the structural and functional properties of starch-based edible films. Polymers 10. https://doi.org/10.3390/polym10040412.

Boutchuen, A., Zimmerman, D., Aich, N., Masud, A.M., Arabshahi, A., Palchoudhury, S., 2019. Increased plant growth with hematite nanoparticle fertilizer drop and determining nanoparticle uptake in plants using multimodal approach. J. Nanomater. 1–11. https://doi.org/10.1155/2019/6890572, 2019.

Bradford, M.M., 1976. A rapid and sensitive method for the quantitation of microgram quantities of protein utilizing the principle of protein-dye binding. Anal. Biochem. 72, 248–254. https://doi.org/10.1006/abio.1976.9999.

Chhikara, N., Kushwaha, K., Sharma, P., Gat, Y., Panghal, A., 2019. Bioactive compounds of beetroot and utilization in food processing industry: a critical review. Food Chem. 272, 192–200.

de França Bettencourt, G.M., Degenhardt, J., Torres, L.A.Z., de Andrade Tanobe, V.O., Soccol, C.R., 2020. Green biosynthesis of single and bimetallic nanoparticles of iron and manganese using bacterial auxin complex to act as plant bio-fertilizer. Biocatal. Agric. Biotechnol. 30, 101822. https://doi.org/10.1016/j.bcab.2020.101822.

Dimkpa, C.O., Singh, U., Adisa, I.O., Bindraban, P.S., Elmer, W.H., Gardea-Torresdey, J.L., White, J.C., 2018. Effects of manganese nanoparticle exposure on nutrient acquisition in wheat (Triticum aestivum L.). Agronomy 8, 158. https://doi.org/10.1016/j.bcab.2016.06.004.

Elmer, W.H., White, J.C., 2016. The use of metallic oxide nanoparticles to enhance growth of tomatoes and eggplants in disease infested soil or soilless medium. Environ. Sci.: Nano 3, 1072–1079. https://doi.org/10.1039/c6en00146g.

Fatima, F., Hashim, A., Anees, S., 2021. Efficacy of nanoparticles as nanofertilizer production: a review. Environ. Sci. Pollut. Control Ser. 28 (2), 1292–1303. https://doi.org/10.1007/s11356-020-11218-9.

Fouad, A.S., Hafez, R.M., 2018. Effect of cobalt nanoparticles and cobalt ions on alkaloids production and expression of CrMPK3 gene in Catharanthu sroseus suspension cultures. Cell. Mol. Biol. 64, 62. https://doi.org/10.14715/cmb/2018.64.12.13.

Gökmen, V., Bahçeci, S., Acar, J., 2002. Characterization of crude lipoxygenase extract from green pea using a modified spectrophotometric method. Eur. Food Res. Technol. 215, 42–45. https://doi.org/10.1007/s00217-002-0518-x.

Hamza, E.M., 2019. Improvement of potato micropropagation and microtubers formation as affected by nanoparticles. Middle East J. 8, 525–532.

Hill, D., Nelson, D., Hammond, J., Bell, L., 2021. Morphophysiology of potato (Solanum tuberosum) in response to drought stress: paving the way forward. Front. Plant Sci. 11, 2258. https://doi.org/10.3389/fpls.2020.597554.

Jeyasubramanian, K., Gopalakrishnan, Thoppey, U.U., Hikku, G.S., Selvakumar, N., Subramania, A., Krishnamoorthy, K., 2016. Enhancement in growth rate and productivity of spinach grown in hydroponics with iron oxide nanoparticles. RSC Adv. 6, 15451–15459. https://doi.org/10.1039/c5ra23425e.

Joshi, N., Jain, N., Pathak, A., Singh, J., Prasad, R., Upadhyaya, C.P., 2018. Biosynthesis of silver nanoparticles using Carissa carandas berries and its potential antibacterial activities. J. Sol. Gel Sci. Technol. 86, 682–689. https://doi.org/10.1007/s10971-018-4666-2.

Joshi, N., Pathak, A., Anupam, R., Jain, N., Singh, J., Upadhyaya, C.P., 2019. A rapid and efficient biosynthesis of metallic nanoparticles using aqueous extract of Chia (Salvia hispanicaL.) seeds. Bionanoscience 9 (4), 893–902. https://doi.org/10.1007/s12668-019-00672-6.

Karunakaran, G., Jagathambal, M., Van Minh, N., Kolesnikov, E., Gusev, A., Zakharova, O.V., Scripnikova, E.V., Vishnyakova, E.D., Kuznetsov, D., 2017. Green synthesized iron oxide nanoparticles: a nano-nutrient for the growth and enhancement of flax (*Linumus itatissimum* L). Plant Int. J. Biotechnol. Bioeng. 11 (4) https://doi.org/10.5281/zenodo.1129910.

Khalil, A.T., Hameed, S., Afridi, S., Mohamed, H.E., Shinwari, Z.K., 2021. Sageretia thea mediated biosynthesis of metal oxide nanoparticles for catalytic degradation of crystal violet dye. Mater. Today 36 (1), 397–400. https://doi.org/10.1016/j.matpr.2020.04.687.

Khan, M.N., Mobin, M., Abbas, Z.K., AlMutairi, K.A., Siddiqui, Z.H., 2017. Role of nanomaterials in plants under challenging environments. Plant Physiol. Biochem. PPB 110, 194–209. https://doi.org/10.1016/j.plaphy.2016.05.038.

Khan, S.A., Shahid, S., Shahid, B., Fatima, U., Abbasi, S.A., 2020. Green synthesis of MnO nanoparticles using abutilon indicum leaf extract for biological, photocatalytic, and adsorption activities. Biomolecules 10 (5), 785. https://doi.org/10.3390/biom10050785.

Koda, Y., 1997. Possible involvement of jasmonates in various morphogenic events. Physiol. Plantarum 100, 639–646. https://doi.org/10.1111/j.1399-3054.1997.tb03070.x.

Kolomiets, M.V., Hannapel, D.J., Chen, H., Tymeson, M., Gladon, R.J., 2001. Lipoxygenase is involved in the control of potato tuber development. Plant Cell 13, 613–626. https://doi.org/10.1105/tpc.13.3.613.

Liu, W., Zeb, A., Lian, J., Wu, J., Xiong, H., Tang, J., Zheng, S., 2020. Interactions of metal-based nanoparticles (MBNPs) and metal-oxide nanoparticles (MONPs) with crop plants: a critical review of research progress and prospects. Environ. Rev. 28 (3), 294–310. https://doi.org/10.1139/er-2019-0085.

Marslin, G., Sheeba, C.J., Franklin, G., 2017. Nanoparticles alter secondary metabolism in plants via ros burst. Front. Plant Sci. 8, 832. https://doi.org/10.3389/fpls.2017.00832.

Mirzajani, F., Askari, H., Hamzelou, S., Schober, Y., Rompp, A., Ghassempour, A., Spengler, B., 2014. Proteomics study of silver nanoparticles toxicity on *Oryza sativa* L. Ecotoxicology Environ saf 108, 335–339. https://doi.org/10.1016/j.ecoenv.2014.07.013.

Moradbeygi, H., Jamei, R., Heidari, R., Darvishzadeh, R., 2020. Fe_2O_3 nanoparticles induced biochemical responses and expression of genes involved in rosmarinic acid biosynthesis pathway in Moldavian balm under salinity stress. Physiol. Plantarum 169 (4), 555–570. https://doi.org/10.1111/ppl.13077.

Mourdikoudis, S., Pallares, R.M., Thanh, N.T., 2018. Characterization techniques for nanoparticles: comparison and complementarity upon studying nanoparticle properties. Nanoscale 10 (27), 12871–12934. https://doi.org/10.1039/C8NR02278J.

Mozafari, A., Havas, F., Ghaderi, N., 2018a. Application of iron nanoparticles and salicylic acid in in vitro culture of strawberries (Fragaria × ananassa Duch.) to cope with drought stress. Plant Cell Tissue Organ Cult. 132 https://doi.org/10.1007/s11240-017-1347-8.

Mozafari, A.A., Ghadakchi, A.A., Ghaderi, N., 2018b. Grape response to salinity stress and role of iron nanoparticle and potassium silicate to mitigate salt induced damage under in vitro conditions Physiology and molecular biology of plants. Int. J. Funct. Plant Biol. 24, 25–35. https://doi.org/10.1007/s12298-017-0488-x.

Murashige, T., Skoog, F., 1962. A revised medium for rapid growth and bio assays with tobacco tissue cultures. Physiol. Plantarum 15, 473–497. https://doi.org/10.1111/j.1399-3054.1962.tb08052.x.

Nam, K.-H., Minami, C., Kong, F., Matsuura, H., Takahashi, K., Yoshihara, T., 2005. Relation between environmental factors and the lox activities upon potato tuber formation and flower-bud formation in morning glory. Plant Growth Regul. 46, 253–260. https://doi.org/10.1007/s10725-005-0056-1.

Nazri, M.K.H.M., Sapawe, N., 2020. A short review on green synthesis of iron metal nanoparticles via plants extracts Materials Today. In: Proceedings. https://doi.org/10.1016/j.matpr.2020.10.968.

Palchoudhury, S., et al., 2018. Enhanced legume root growth with pre-soaking in α-Fe_2O_3 nanoparticle fertilizer. RSC Adv. 8, 24075–24083. https://doi.org/10.1039/c8ra04680h.

Pradhan, S., et al., 2013. Photochemical modulation of biosafe manganese nanoparticles on Vignaradiata: a detailed molecular, biochemical, and biophysical study. Environ. Sci. Technol. 47, 13122–13131. https://doi.org/10.1021/es402659t.

Rastogi, A., Zivcak, M., Sytar, O., Kalaji, H.M., He, X., Mbarki, S., Brestic, M., 2017. Impact of metal and metal oxide nanoparticles on plant: a critical review. Front. Chem. 5, 78. https://doi.org/10.3389/fchem.2017.00078.

Rizwan, M., Ali, S., Ali, B., Adrees, M., Arshad, M., Hussain, A., Rehman, M.Z., Waris, A.A., 2019. Zinc and iron oxide nanoparticles improved the plant growth and reduced the oxidative stress and cadmium concentration in wheat. Chemosphere 1 (214), 269–277. https://doi.org/10.1016/j.chemosphere.2018.09.120.

Rui, M., et al., 2016. Iron oxide nanoparticles as a potential iron fertilizer for peanut (Arachis hypogaea). Front. Plant Sci. 7, 815. https://doi.org/10.3389/fpls.2016.00815.

Sanzari, I., Leone, A., Ambrosone, A., 2019. Nanotechnology in plant science: to make a long story short. Front. Bioeng. Biotechnol. 7, 120. https://doi.org/10.3389/fbioe.2019.00120.

Saratale, R.G., Saratale, G.D., Shin, H.S., Jacob, J.M., Pugazhendhi, A., Bhaisare, M., Kumar, G., 2018. New insights on the green synthesis of metallic nanoparticles using plant and waste biomaterials: current knowledge, their agricultural and environmental applications. Environ. Sci. Pollut. Res. 25, 10164–10183. https://doi.org/10.1007/s11356-017-9912-6.

Seifu, Y.W., Deneke, S., 2017. Effect of calcium chloride and calcium nitrate on potato (Solanum tuberosum L.) growth and yield. J. Hortic. For. 4, 207. https://doi.org/10.4172/2376-0354.1000207.

Shankramma, K., Yallappa, S., Shivanna, M., Manjanna, J., 2016. Fe2O3 magnetic nanoparticles to enhance S. lycopersicum (tomato) plant growth and their biomineralization. Appl. Nanosci. 6, 983–990. https://doi.org/10.1007/s13204-015-0510-y.

Shi, Y., Li, J., Sun, Z., 2020. Success to iron biofortification of wheat grain by combining both plant and microbial genetics. Rhizosphere 15 (1), 100218. https://doi.org/10.1016/j.rhisph.2020.100218.

Sidhu, M.K., Raturi, H.C., Kachwaya, D.S., Sharma, A., 2019. Role of micronutrients in vegetable production: a. J. Pharmacogn. Phytochem. 1, 332–340.

Singh, J., Dutta, T., Kim, K.H., et al., 2018. 'Green' synthesis of metals and their oxide nanoparticles: applications for environmental remediation. J. Nanobiotechnol. 16, 84. https://doi.org/10.1186/s12951-018-0408-4.

Singh, J., Kumar, S., Alok, A., Upadhyay, S.K., Rawat, M., Tsang, D.C.W., Bolan, N., Kim, K., 2019. The potential of green synthesized zinc oxide nanoparticles as nutrient source for plant growth. J. Clean. Prod. 214, 1061–1070. https://doi.org/10.1016/j.jclepro.2019.01.018.

Souri, M., Hoseinpour, V., Shakeri, A., Ghaemi, N., 2018. Optimization of green synthesis of MnO nanoparticles via utilizing response surface methodology. IET Nanobiotechnol. 12, 822–827. https://doi.org/10.1049/iet-nbt.2017.0145.

Tariq, A., Ilyas, S., Naz, S., 2020. Nanotechnology and plant tissue culture. In: Javad, S. (Ed.), Nanoagronomy. Springer, Cham. https://doi.org/10.1007/978-3-030-41275-32.

Umavathi, S., Mahboob, S., Govindarajan, M., Al-Ghanim, K.A., Ahmed, Z., Norah Al-Mulhm, P.V., Kasi, Gopinath, M.S., Kavitha, C., 2021. Green synthesis of ZnO nanoparticles for antimicrobial and vegetative growth applications: a novel approach for advancing efficient high quality health care to human wellbeing. Saudi J. Biol. Sci. 28 (3), 1808–1815. https://doi.org/10.1016/j.sjbs.2020.12.025.

Upadhyaya, C.P., Bagri, D.S., Upadhyaya, D.C., Pathak, A.K., Kawar, P.G., 2016. Molecular and biochemical analysis of supplementation of calcium under in vitro condition on tuberization in potato (Solanum tuberosum L.). Biocatal. Agric. Biotechnol. 7, 210–216. https://doi.org/10.1016/j.bcab.2016.06.004.

Upadhyaya, C.P., Gururani, M.A., Prasad, R., Verma, A., 2013. A cell wall extract from Piriformosporaindica promotes tuberization in potato (Solanum tuberosum L.) via enhanced expression of Ca (+2) signaling pathway and lipoxygenase gene. Appl. Biochem. Biotechnol. 170, 743–755. https://doi.org/10.1007/s12010-013-0231-1.

Vincenti, S., Mariani, M., Alberti, J.C., Jacopini, S., Brunini-Bronzini, de-Caraffa, V., Berti, L., Maury, J., 2019. Biocatalytic synthesis of natural green leaf volatiles using the lipoxygenase metabolic pathway. Catalysts 9 (10), 873. https://doi.org/10.3390/catal9100873.

Yan, A., Chen, Z., 2018. Detection methods of nanoparticles in plant tissues. New Visions in Plant Science 19, 99.

Zhao, L., Lu, L., Wang, A., Zhang, H., Huang, M., Wu, H., Xing, B., Wang, Z., Ji, R., 2020. Nano-biotechnology in agriculture: use of nanomaterials to promote plant growth and stress tolerance. J. Agric. Food Chem. 68 (7), 1935–1947.